Dimerization Paths of CH_2 and SiH_2 Fragments to Ethylene, Disilene, and Silaethylene: MCSCF and MRCI Study of Least- and Non-Least-Motion Paths

Katsuhisa Ohta, Ernest R. Davidson,[1] and Keiji Morokuma*

Contribution from The Institute for Molecular Science, Myodaiji, Okazaki 444, Japan.
Received December 4, 1984

Abstract: Dimerization of CH_2 and SiH_2 in both singlet and triplet states is investigated by MCSCF and MRCI in connection with the least-motion path vs. the non-least-motion path. Two ground-state ($^3B_1$) methylenes in the non-least-motion path give a ground-state ethylene without barrier. The ground-state ($^1A_1$) silylenes give a ground-state disilene with barrier in the least-motion path and without barrier in the non-least-motion path. As a mixed system, silaethylene is also investigated. A ground-state ($^3B_1$) methylene and an excited-state ($^3B_1$) silylene give a ground-state silaethylene without barrier in the least-motion path, and an excited-state methylene ($^1A_1$) and a ground-state ($^1A_1$) silylene also give a ground-state silaethylene without barrier in the non-least-motion path.

Dimerization of singlet methylenes to form a ground-state ethylene had been considered as a textbook example for the non-least-motion reaction path. In the least-motion path (D_{2h}) four valence electrons, originally two in the σ orbital of a CH_2 unit (σ_A) and two in the σ orbital in the other CH_2 unit (σ_B), have to fill a σ_g and a π_u orbital in ethylene, and $\sigma_A^2\sigma_B^2 \rightarrow \sigma_g^2\pi_u^2$ is symmetry forbidden. In a non-least-motion path proposed by Hoffmann, Gleiter, and Mallory (hereafter referred as HGM),[2] the reaction path starts with a C_s symmetry, mixing σ and π orbitals and making the process symmetry allowed, and then takes a higher symmetry of D_{2h} in a later stage of reaction. This argument, however, is based on an extended Hückel method, i.e., a single determinant wave function, which is insufficient to describe essential electronic configurations. Moreover, the ground state of CH_2 is a triplet,[3] $^3B_1$, and the above argument does not apply to dimerization of triplets.

Recent ab initio calculations have shown that two ground-state triplet methylenes can dimerize via the least-motion path without barrier to give the ground-state ethylene.[4] On the other hand two singlet methylenes dimerize via the least-motion path to give a Rydberg excited state of ethylene.[5] A conclusion is that methylene dimerization is not a good example of non-least-motion reaction.

There remain several questions to be answered. Here, we have studied dimerization of singlet methylenes and triplet methylenes via a non-least-motion path. Is there a barrier along the HGM non-least-motion path? What is the state formed in the non-least-motion dimerization of methylenes? We have also studied dimerization of triplet and singlet silylene (SiH_2) both via the least-motion and a non-least-motion path. The ground state of silylene is a singlet, $^1A_1$, and the lowest triplet $^3B_1$ is the first excited state, opposite to the case of methylene. The coupling reaction of CH_2 and SiH_2 to give silaethylene CH_2SiH_2 via the least-motion and a non-least-motion path has also been investigated.

Method of Calculation

The basis set used in this study consists of the Dunning-Hay contracted Gaussian functions,[6] [3s2p] on carbon, [6s4p] on silicon, and [2s] on hydrogen, augmented with the polarization d functions ($\alpha_d = 0.75$ for carbon[6] and 0.60 for silicon[7a]). In the calculation of CH_2CH_2, a set of diffuse basis functions ($\alpha_s = 0.023$ and $\alpha_p = 0.021$)[6] describing Rydberg states was also added to carbon atoms. The number of basis functions is 19 (without Rydberg AO's) or 23 (with Rydberg AO's) for CH_2 and 28 for SiH_2. For CH_2CH_2, the HGM non-least-motion path was adopted and extended, as described later. For SiH_2SiH_2 and CH_2SiH_2 the non-least-motion paths were determined with the Hartree-Fock-Roothaan (HFR) energy gradient with the GAUSSIAN80[8] program, by minimizing the energy at several Si-Si or C-Si distances, respectively, with respect to all the other degrees of freedom. Potential curves were obtained with the MCSCF wave function with the GAMESS[9] program along the least-motion and the above determined non-least-motion paths. The MCSCF wave function is of 4-electron/4-orbital complete active space (CAS) type and the number of electronic configurations is 20 in the C_s symmetry. Four active orbitals are σ, π, π^*, and σ^* in the least-motion path (D_{2h} for CH_2CH_2 and SiH_2SiH_2, and C_{2v} for CH_2SiH_2) and their mixtures (all in a' symmetry in C_s) in the non-least-motion path. Along the non-least-motion path of CH_2CH_2 we also calculated multireference CI (MRCI) energy by the use of the MELD[10] program, where orbitals obtained by the MCSCF calculation were used and all the single and double excitations (6332 spin-adapted configurations) from the four active orbitals to all virtual orbitals were included.

CH_2 and SiH_2 Fragments

(A) CH_2. The geometries for the first $^3B_1$ and $^1A_1$ states were optimized with the open-shell HFR[11] and the 2-electron/2-orbital (and 2-electron/3-orbital) CAS MCSCF wave function, respectively. The optimized geometry for each state and the energies of both states at optimized geometries are given in Table I with other theoretical[12,13] and experimental[14-16] results. The optimum HCH bond angle is 128.7° for $^3B_1$ and 103.2° for $^1A_1$ without the Rydberg basis functions, and these diffuse basis functions do not have any significant effect on either energy or geometry of the ground state. The bond angle for the $^3B_1$ state is calculated

(1) Present address: Department of Chemistry, Indiana University, Bloomington, Indiana 47405.
(2) Hoffmann, R.; Gleiter, R.; Mallory, F. B. *J. Am. Chem. Soc.* **1970**, *92*, 1460.
(3) (a) Herzberg, G.; Johns, J. W. C. *J. Chem. Phys.* **1971**, *54*, 2276. (b) Borden, W. T. "Diradicals"; John Wiley and Sons: New York, 1982.
(4) (a) Basch, H. *J. Chem. Phys.* **1971**, *55*, 1700. (b) Cheung, L. M.; Sundberg, K. R.; Ruedenberg, K. *Int. J. Quantum Chem.* **1979**, *16*, 1103. (c) Ruedenberg, K.; Schmidt, M. W.; Gilbert, M. M.; Elbert, S. T. *Chem. Phys.* **1982**, *71*, 41.
(5) Feller, D.; Davidson, E. R. *J. Phys. Chem.* **1983**, *87*, 2721.
(6) Dunning, T. H., Jr.; Hay, D. J. "Modern Theoretical Chemistry"; Schaefer, H. F., III, Ed.; Plenum Press: New York, 1977.
(7) (a) Yoshioka, Y.; Goddard, J. D.; Schaefer, H. F., III *J. Am. Chem. Soc.* **1981**, *103*, 2452. (b) Sachaefer, H. F., III *Acc. Chem. Res.* **1982**, *15*, 283. (c) Bernardi, F.; Robb, M. A. *Mol. Phys.* **1983**, *48*, 1345.
(8) Binkley, J. S.; Whiteside, R. A.; Krishnan, R.; Seeger, R.; DeFrees, D. J.; Schlegel, H. B.; Topiol, S.; Kahn, L. R.; Pople, J. A., program 406 in Quantum Chemistry Program Exchange Catalogue 13 (Indiana University, Bloomington, 1981).
(9) Dupuis, M.; Spangler, D.; Wendoloski, J. J. NRCC Software Catalog, 1980, Vol. 1, Program No. QG01.
(10) Davidson, E. R.; McMurchie, L.; Elbert, S.; Langhoff, S.; Rawlings, D.; Feller, D. (Quantum Chemistry Group, University of Washington).
(11) The result of 2-electron/2-orbital MCSCF for $^3B_1$ is exactly the same as that of open-shell RHF in the case of CH_2 or SiH_2.
(12) (a) Harding, L. B.; Goddard, W. A., III *Chem. Phys. Lett.* **1978**, *55*, 217. (b) Shih, S.; Peyerimhoff, S. D.; Buenker, R. J.; Feric, M. *Chem. Phys. Lett.* **1978**, *55*, 206.
(13) Rice, J. E.; Handy, N. C. *Chem. Phys. Lett.* **1984**, *107*, 365.
(14) Bunker, P. R.; Jensen, P. *J. Chem. Phys.* **1983**, *79*, 1224.
(15) Herzberg, G.; Johns, J. W. C. *Proc. R. Soc. London, Ser. A* **1966**, *295*, 107.
(16) McKellar, A. R. W.; Bunker, P. R.; Sears, T. J.; Evenson, K. M.; Saykally, R. J.; Langhoff, S. R. *J. Chem. Phys.* **1983**, *79*, 5251.

0002-7863/85/1507-3466$01.50/0

Table I. Geometry and Energy of CH_2

method	state	∠HCH, deg	R(C–H), Å	energy, hartree	ΔE, kcal mol^{-1}	ref
GVB–POLCI	$^3B_1$	133.2	1.084		0.0	12(a)
	$^1A_1$	101.8	1.113		10.4	
MRDCI	$^3B_1$	132.3	1.076	−39.0849	0.0	12b
	$^1A_1$	102.9	1.111		11.1	
MCSCF	$^3B_1$	131.7	1.098		0.0	13
	$^1A_1$	102.0	1.128		9.80	
MC-1 with Rydberg AO[a]	$^3B_1$	128.9	1.073[b]	−38.923938	0.0	this work
		103.2	1.099[c]	−38.909326	9.2	
	$^1A_1$	103.2	1.099[c]	−38.902592	13.4	
		128.9	1.073[b]	−38.886833	23.3	
MC-2 without Rydberg AO[a]	$^3B_1$	128.7	1.074[b]	−38.923812	0.0	this work
		103.2	1.100[c]	−38.909115	9.2	
	$^1A_1$	103.2	1.100[c]	−38.902068	13.6	
		128.7	1.074[b]	−38.886461	23.4	
MC-2 with Rydberg AO[a]	$^3B_1$	120.0	1.100[d]	−38.921619	0.0	this work
	$^1A_1$	120.0	1.100[d]	−38.895309	16.5	
exptl	$^3B_1$	133.8	1.075		0.0	14
	$^1A_1$	102.4	1.11			15
	$^1A_1$				9.05	16

[a] Calculational method is open-shell HFR for $^3B_1$ and 2-electron/3-orbital CAS MCSCF (MC-1) or 2-electron/2-orbital CAS MCSCF (MC-2) for $^1A_1$. [b] Optimum geometry for the $^3B_1$ state. [c] Optimum geometry for the $^1A_1$ state. [d] Geometry of HGM's methylene (ref 2).

Table II. Geometry and Energy of SiH_2

method	state	∠HSiH, deg	R(Si–H), Å	energy, hartree	ΔE, kcal mol^{-1}	ref
MRSDCI	$^1A_1$	93.9	1.505	−290.10268	0.0	18
	$^3B_1$	118.1	1.466		16.8	
MCSCF	$^1A_1$	92.75	1.534	−290.065223	0.0	13
	$^3B_1$	118.3	1.497		17.5	
MCSCF[a]	$^1A_1$	93.9	1.497[b]	−290.013076	0.0	this work
		118.0	1.460[c]	−289.996446	10.4	
	$^3B_1$	118.0	1.460[c]	−289.989313	15.2	
		93.9	1.497[b]	−289.975665	23.5	
exptl	$^1A_1$	92.1	1.516		0.0	19

[a] Calculational method is 2-electron/2-orbital CAS MCSCF for $^1A_1$ and open-shell HFR for $^3B_1$. [b] Optimum geometry for the $^1A_1$ state. [c] Optimum geometry for the $^3B_1$ state.

slightly smaller than the experimental and other theoretical results. The $^3B_1$ state is more stable than the $^1A_1$ state by 13.6 kcal/mol. This is a reasonable value for the level of our calculation in comparison with more accurate theoretical values, 10.4, 11.1, 9.80 kcal/mol, and the experimental value 9.05 kcal/mol. We note that the experimental HCH bond angle 117.6° and C–H bond length 1.086 Å of CH_2CH_2 in the ground state[17] are respectively in between those in the $^3B_1$ state and in the $^1A_1$ state of isolated CH_2. Vertically excited and de-excited states were also calculated. It is estimated by theoretical[12] and experimental[16] studies that the energy of the $^3B_1$ state is very close to that of the $^1A_1$ state at the $^1A_1$ optimum geometry. Here, the $^3B_1$ state is calculated slightly more stable than the $^1A_1$ state at the $^1A_1$ optimum geometry. At the structure of CH_2 fragment used in the HGM non-least-motion path,[2] R(C–H) = 1.10 Å and ∠HCH = 120°, the singlet–triplet energy separation is calculated to be 16.5 kcal/mol. In the following we will adopt this geometry for CH_2 fragments to trace the non-least-motion path to reach CH_2CH_2.

(B) SiH_2. Our interest in the calculation of $SiH_2 + SiH_2$ and $CH_2 + SiH_2$ is to compare the dimerization path with $CH_2 + CH_2$ in the ground state, and, therefore, no Rydberg basis set was augmented on the Si atom. Calculated results for SiH_2 are given in Table II with other theoretical[13,18] and experimental results.[19] The $^1A_1$ state is found to be more stable than the $^3B_1$ by 15.2 kcal/mol, and it is the situation opposite to that of CH_2. The bond angle ∠HSiH in $^1A_1$ is much smaller than that of $^3B_1$. Our results are reasonable in comparison with the experimental and other theoretical results. Vertical excited and de-excited states were also calculated. Even at the optimum geometry for $^3B_1$, the $^1A_1$ state is more stable than the $^3B_1$ state. Recently, Rice and Handy have reported a 6-electron/6-orbital and 6-electron/8-orbital MCSCF study on the ground and lower excited states of SiH_2.[13] The $^1A_1$ state, in their study, is also more stable than the $^3B_1$ state even at the optimum structure for $^3B_1$. Crossing occurs around 130°, an angle larger than either of the two optima.

Thus, there is no crossing of the potential curves along the bond angle coordinate between the bond angle optimum for the triplet state and that for the singlet state. The $^3B_1$ state is always more stable than the $^1A_1$ state in CH_2 and the $^1A_1$ is always more stable than the $^3B_1$ in SiH_2. In the case of CH_2, however, calculations more accurate than ours may be needed for a quantitative discussion of the relative stability of the $^3B_1$ state at the $^1A_1$ optimum geometry.

Non-Least-Motion Dimerization $CH_2 + CH_2 \rightarrow CH_2CH_2$

As discussed in a preceding section, the least motion (D_{2h}) approach in $CH_2 + CH_2$ has already been investigated in some MCSCF calculations.[4,5,7c] Along this path two triplet ($^3B_1$) methylenes form the ground state of ethylene without any barrier. On the other hand, two singlet ($^1A_1$) methylenes do not form the ground state, but go to a Rydberg excited state of ^1A_g symmetry.[5] Concerning the non-least-motion path of dimerization of CH_2 fragments, HGM extended Hückel result was that two singlet

(17) Herzberg, G. "Electronic Spectra of Polyatomic Molecules"; Van Nostrand: Princeton, 1966.
(18) Colvin, M. E.; Grev, R. S.; Schaefer, H. F., III *Chem. Phys. Lett.* **1983**, *99*, 399.
(19) Dubois, I.; Herzberg, G.; Verma, R. D. *J. Chem. Phys.* **1967**, *47*, 4262.

Table III. HGM Non-Least-Motion Path and Its Extention for $CH_2 + CH_2$[a]

R(C–C), Å	ϕ_1,[b] deg	ϕ_2,[b] deg
1.30	0.0	0.0
1.35	0.0	0.0
1.40	0.0	0.0
1.50	0.0	0.0
1.60	0.0	0.0
1.70	0.0	0.0
1.80	0.0	0.0
1.90	0.0	0.0
2.00	0.0	0.0
2.20	16.0	16.0
2.30	27.0	27.0
2.40	34.0	34.0
2.45	37.0	37.0
2.50	54.0	24.0
2.55	62.0	20.0
2.60	67.0	16.0
2.80	78.0	9.0
3.00	84.0	6.0
4.00	89.0	2.0

[a] R(C–H) and ∠HCH are fixed to 1.10 Å and 120°, respectively. [b] ϕ_1 and ϕ_2 are the bending angles from the C–C axis to the trans form in C_s or C_{2h} structure.

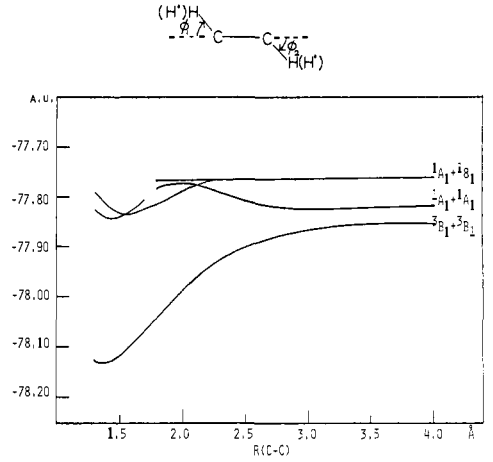

Figure 1. Potential curves for dimerization of CH_2 along the HGM non-least-motion path as a function of R(C–C). MRCI calculations with MCSCF orbitals.

methylenes formed the ground ^1A_g state of ethylene with no barrier. In the following, we study the CH_2 dimerization process in both the ground and lower excited states along the HGM non-least-motion path, using correlated wave functions needed to describe the process properly. We have used the non-least-motion path determined by HGM and augmented it with a few more points at a short C–C distance in D_{2h} symmetry, as given in Table III. At the far end of this path where the overall symmetry is C_s, one CH_2 has its C_{2v} axis nearly parallel to the line of approach whereas the other CH_2 has its C_{2v} axis nearly perpendicular to the line of approach. At 2.45 Å of C–C separation, the bending angles of two CH_2 units become equal with an overall C_{2h} symmetry and a trans conformation. At 2.00 Å the bending angles become zero and the entire system is planar (D_{2h}). The HGM D_{2h} path was extended from 2.00 to 1.30 Å, in order to trace the reaction to completion. The structure of CH_2 fragments are fixed at R(C–H) = 1.10 Å and ∠HCH = 120° throughout the path.

In Figure 1 the potential energy curves along the non-least-motion path for the ground and some excited states are shown. Two triplet ($^3B_1$) methylenes approach each other on the ground-state singlet curve and without barrier go to the ground state of ethylene. The situation is essentially the same with the least-motion dimerization, but different from the HGM results where two *singlet* ($^1A_1$) methylenes are to form the ground-state ethylene. The dimerization of two singlet ($^1A_1$) methylenes in

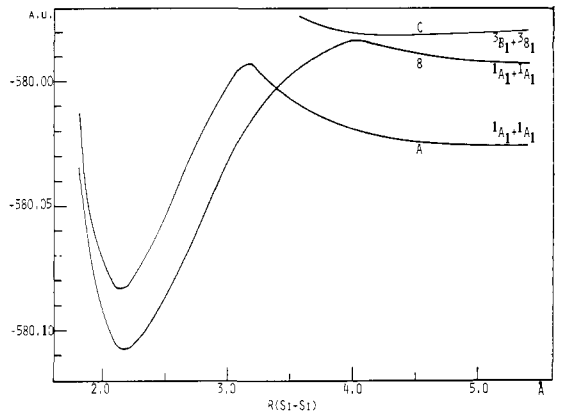

Figure 2. Potential curves for dimerization of SiH_2 along the least-motion path. ∠HSiH and R(Si–H) are fixed to 93.9° and 1.497 Å for curve A and 118.0° and 1.460 Å for curves B and C, respectively. MCSCF calculations.

Figure 1 follows the first excited state, which is a valence excited state at long distance, goes over a barrier caused by avoided crossing, and becomes a Rydberg excited state of ethylene. This situation is again similar to the case of the least-motion path. The third and fourth states both represent the dimerization of $CH_2(^1A_1) + CH_2(^1B_1)$ or $CH_2(^1B_1) + CH_2(^1A_1)$. They are nearly degenerate up to around 2.3 Å, inside of which the lower state without barrier forms an excited ethylene.

Dimerization $SiH_2 + SiH_2 \rightarrow SiH_2SiH_2$

There are few ab initio calculations about disilene,[20] and there is some confusion on the ground-state conformation whether it is planar (D_{2h}) or trans (C_{2h}). The calculated energy difference between planar and trans conformation is, however, found to be very small. In Table IV, the optimized geometry by HFR is given for D_{2h} and C_{2h} structures. In our results, the trans form is slightly more stable than the planar structure by 0.08 kcal/mol in the HFR calculation. In the following study on the dimerization path of two SiH_2 fragments, this small energy difference in the vicinity of the equilibrium structure is not so important. One notes that the HSiH bond angle and Si–H bond length of disilene are very close to those of SiH_2 in the $^3B_1$ state in Table II.

(A) Along the Least-Motion Path. Figure 2 shows three potential energy curves for overall singlet states for the dimerization of SiH_2 along the least-motion path. In curve A, the Si–H distance and the HSiH angle are fixed at the calculated values for the $^1A_1$ ground state of SiH_2, i.e., 1.497 Å and 93.9°, respectively. This curve thus represents the dimerization of singlet silylenes in the least-motion path. Figure 2 and the analysis of the wave function indicate that in the first half of the dimerization reaction the potential curve is repulsive as the Si–Si distance decreases, and the total singlet wave function consists mainly, as expected, of a product of σ^2 singlet wave functions of the reactants. Around 3.1 Å the triplet ($\sigma\pi$) × triplet ($\sigma\pi$) configuration takes over, which is attractive and leads to the ground-state disilene. The barrier is caused by avoided crossing between these two major configurations and is a typical example of symmetry-forbidden reactions.

Both curves B and C assume the Si–H distance and HSiH angle fixed at the calculated values for $^3B_1$ SiH_2, i.e., 1.460 Å and 118.0°, respectively. In our calculation of SiH_2 even at this geometry the singlet is lower in energy than the triplet. Therefore, the lower curve B, as in curve A, consists mainly of a singlet × singlet configuration and becomes a triplet × triplet inside the barrier due to avoided crossing around 4.0 Å. The barrier is earlier in curve B than in curve A, because the assumed fragment geometries in curve B are more favorable to the triplet × triplet configuration than the singlet × singlet configuration. The upper curve C represents the least-motion path for dimerization of $^3B_1$ silylenes. The triplet × triplet wave function at a long distance goes through

(20) (a) Poirier, R. A.; Goddard, J. D. *Chem. Phys. Lett.* **1981**, *80*, 37. (b) Lischka, H.; Kohler, H. J. *Chem. Phys. Lett.* **1982**, *85*, 467.

Table IV. Geometry and Energy of SiH_2SiH_2

state	R(Si–Si), Å	R(Si–H), Å	∠HSiH, deg	ϕ,[a] deg	energy, hartree	ΔE, kcal mol^{-1}
^1A_g (D_{2h})	2.119	1.456	115.6	0.0	−580.070185	0.00
					−580.106834[b]	0.00
^1A_g (C_{2h})	2.127	1.456	114.7	15.6	−580.070312	−0.08
					−580.107944[b]	−0.71

[a] ϕ is the bending angle from the Si–Si axis to the trans form. [b] 4-Electron/4-orbital CAS MCSCF energy calculated at HFR optimized geometry.

Table V. Non-Least-Motion Path of SiH_2SiH_2[a,b]

R(Si–Si), Å	ϕ_1, deg	θ_1, deg	R_1(Si–H), Å	ϕ_2, deg	θ_2, deg	R_2(Si–H), Å
2.127	15.6	114.7	1.456	15.6	114.7	1.456
2.40	15.0	109.7	1.463	39.4	108.8	1.469
2.60	14.5	106.1	1.468	56.9	104.5	1.478
2.80	14.0	102.5	1.474	74.3	100.1	1.487
3.00	13.5	98.8	1.479	91.7	95.8	1.496
3.40	3.5	96.7	1.485	97.9	94.2	1.499
3.80	0.4	95.5	1.489	99.6	93.8	1.498
4.20	0.2	94.8	1.492	99.5	93.7	1.497

[a] ϕ_1 is the bending angle of the SiH_2 fragment in the left-hand side and ϕ_2 is that of the other fragment to the trans form.

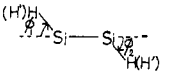

θ_1 is the HSiH bond angle of the left-hand side SiH_2 fragment and θ_2 is that of the other SiH_2 fragment. R_1(Si–H) is the SiH bond length of the left-hand fragment and R_2(Si–H) is that of the other fragment. [b] The geometrical parameters at R(Si–Si) = 2.40, 2.60, and 2.80 Å are not optimized by HFR energy gradient but obtained by linear interpolation between 2.127 and 3.00 Å.

Table VI. Geometry and Energy of CH_2SiH_2

state	R(C–Si), Å	R(C–H), Å	∠HCH, deg	R(Si–H), Å	∠HSiH, deg	energy, hartree
^1A_g (C_{2v})	1.692	1.077	114.8	1.455	114.3	−329.044427
						−329.093355[a]

[a] 4-Electron/4-orbital CAS MCSCF energy calculated at HFR optimized geometry.

an avoided crossing with curve B and is adiabatically correlated to an excited state of disilene.

(B) **Along the Non-Least-Motion Path.** An "approximate" non-least-motion path for dimerization of singlet SiH_2 was determined by HFR optimization of geometrical parameters as functions of the Si–Si distance and is listed in Table V. The geometrical parameters were interpolated linearly between R(Si–Si) = 2.127 and 3.00 Å because of the difficulty of convergence of geometry optimization. This difficulty comes from the inadequacy of the single determinant wave function around the avoided crossing region, and the non-least-motion path determined here may not be energitically the best path. Our interest is, however, to prove the existance of a non-least-motion path along which two silylenes dimerize without a barrier. The interpolation is also not a serious problem for the same reason. The energy along this approximate path is calculated with a more reliable 4-electron/4-orbital CAS MCSCF wave function. In an early stage SiH_2 units have singlet-like structure, one of them having its C_{2v} axis nearly parallel and the other perpendicular to the line of approach. In the final stage two SiH_2 units have triplet-like structure, the trans bending angles becoming small and equal. The MCSCF potential energy curve is shown in Figure 3. There is no barrier along this path starting from singlet silylenes.

In conclusion, the ground-state singlet SiH_2 dimerizes to form the ground state of disilene, without barrier on the non-least-motion path and with substantial barrier on the least-motion path. Therefore, HGM's conclusion is found to be applicable to this case of SiH_2 dimerization. The excited-state triplet SiH_2 is adiabatically led to an excited state of disilene, but actually it is likely to form ground-state disilene with no barrier through nonadiabatic transition in the least-motion path. If the triplet silylene happens to be lower in energy than the singlet silylene at the optimum geometry of the triplet, nonadiabatic transition will not be needed and the least-motion path will give the ground-state product without barrier.

Cross-Coupling $CH_2 + SiH_2 \rightarrow CH_2SiH_2$

In this mixed system the Rydberg basis set was not added on the carbon atom, since only the dimerization path in the ground

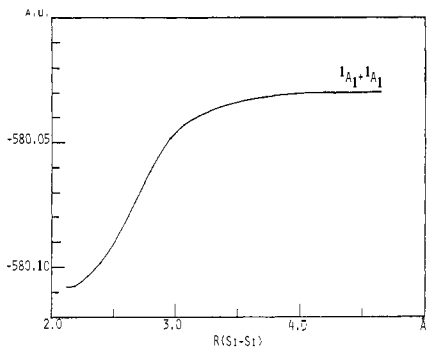

Figure 3. Potential curve for dimerization of SiH_2 ($^1A_1$) along the non-least-motion path as a function of R(Si–Si). An MCSCF calculation.

state was studied. In Table VI, the geometry of CH_2SiH_2 optimized by HFR is given. The stable structure is planar C_{2v}.[7] The bond angle ∠HSiH in CH_2SiH_2 is very near to that of the isolated SiH_2 fragment in $^3B_1$, while the bond angle ∠HCH is about the average value of those in $^3B_1$ and $^1A_1$ states of CH_2.

(A) **Along the Least-Motion Path.** At the infinite separation of this mixed system, our calculations give the total energy of the singlet pairs slightly lower in energy than the triplet pairs. Therefore, as shown in Figure 4, the lowest least-motion path is curve A, where the fragment geometries are fixed at the optimum values for CH_2 ($^1A_1$) and SiH_2 ($^1A_1$). Curve A is repulsive, as all the least motion singlet × singlet curves are, and goes over a large barrier around 3.2 Å to reach the ground-state product. In curves B and C, the fragment geometries are frozen at the values in the equilibrium geometry of silaethylene CH_2SiH_2, which are not too far from those in the triplet fragments. The lowest curve B essentially describes the least-motion reaction for triplet pairs, which with no barrier reaches the ground-stage silaethylene. Curve C starts from distorted two-singlet pairs and is very repulsive.

(B) **Along the Non-Least-Motion Path.** The non-least-motion path of CH_2SiH_2 determined by HFR geometry optimization as a function of C–Si distance is listed in Table VII. Figure 5 shows

Table VII. Non-Least-Motion Path of CH_2SiH_2[a]

R(C-Si), Å	ϕ_1, deg	θ_1, deg	R_1(C-H), Å	ϕ_2, deg	θ_2, deg	R_2(Si-H), Å
1.692	0.0	114.8	1.077	0.0	114.3	1.455
2.00	17.5	117.0	1.076	21.6	115.2	1.453
2.40	28.8	110.6	1.085	73.0	101.2	1.483
2.60	11.5	109.0	1.088	91.0	96.8	1.495
2.80	4.8	107.8	1.089	96.3	95.2	1.498
3.00	2.0	106.8	1.091	98.3	94.4	1.499
3.20	0.6	106.2	1.092	99.3	94.1	1.499
3.60	0.4	105.4	1.094	99.5	93.8	1.498
4.00	0.4	104.8	1.095	99.5	93.8	1.498
5.00	0.3	104.2	1.096	98.7	93.5	1.497

[a] ϕ_1 is the bending angle of the CH_2 fragment from the C–Si axis and ϕ_2 is that of the SiH_2 fragment to the trans form.

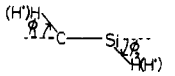

θ_1 is the HCH bond angle of the CH_2 fragment and θ_2 is the HSiH bond angle of the SiH_2 fragment. R_1(C-H) is the C-H bond length and R_2(Si-H) is the Si-H bond length.

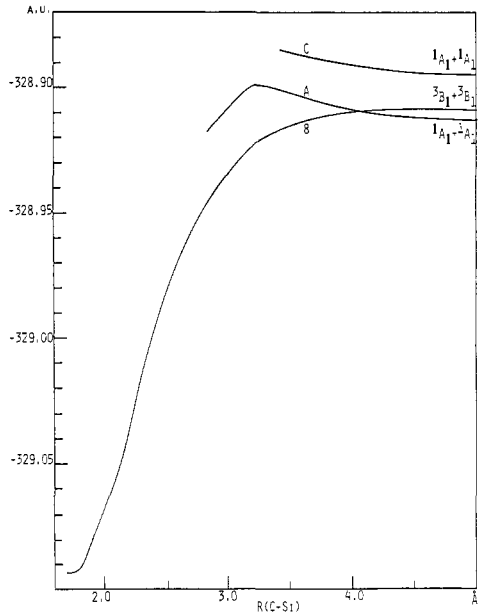

Figure 4. Potential curves for the cross coupling between CH_2 and SiH_2 along the least-motion path. ∠HSiH, R(Si-H), ∠HCH, and R(C-H) are fixed to 93.9°, 1.497 Å, 103.2°, and 1.100 Å for curve A and to 114.3°, 1.455 Å, 114.8°, and 1.077 Å for curves B and C, respectively. MCSCF calculations.

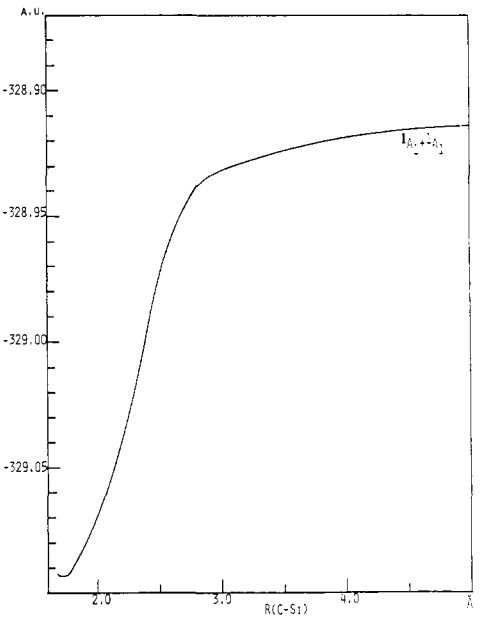

Figure 5. Potential curve for the cross coupling between CH_2 ($^1A_1$) and SiH_2 ($^1A_1$) along the non-least-motion path as a function of R(C-Si). An MCSCF calculation.

the potential energy curve obtained by MCSCF along this non-least-motion path. The singlet pairs form the ground-state product without barrier.

One interesting point to note is that in the early stage of non-least-motion path the preferred geometry has the SiH_2 plane nearly perpendicular to the line of approach and the CH_2 plane nearly parallel to the line, as if SiH_2 is acting as an electron acceptor and CH_2 as an electron donor. An analysis reveals that in the early stage of reaction the electrostatic interaction is dominant and it is most favorable to have a large CH_2 dipole aligned parallel to the line of approach.[21]

(21) Energy decomposition analysis (Kitaura, K.; Morokuma, K. *Int. J. Quantum Chem.* **1976**, *10*, 325) with the HFR wave function was carried out at two conformations of silaethylene. Geometries of SiH_2 and CH_2 fragments are fixed at the optimum values for the isolated SiH_2 ($^1A_1$) and CH_2 ($^1A_1$) states, respectively, and the Si–C distance was fixed at 5.0 Å. In the first conformation, the SiH_2 plane is perpendicular to the Si–C axis and the CH_2 plane is parallel to the axis. In the second conformation, the SiH_2 plane is parallel to the Si–C axis and the CH_2 plane is perpendicular to the Si–C axis. The first conformation was calculated more stable than the second conformation. The stabilization energy is 1.3 kcal/mol for the first conformation and 0.4 kcal/mol for the second case. EDA shows that the dominant component of the stabilization energy was analyzed to the the electrostatic interaction energy, 1.2 kcal/mol for the first case and 0.3 kcal/mol for the second. It is more favorable to have a large CH_2 dipole alligned parallel to the Si–C axis in the long Si–C distance region.

Discussion and Conclusions

We have investigated in detail the dimerization reaction paths of CH_2 and SiH_2 to CH_2CH_2, SiH_2SiH_2, and CH_2SiH_2. A single determinant wave function is not enough to describe the essential electronic structure in these dimerization reactions. A simple estimation based on the orbital symmetry rule has broken down in the case of dimerization of CH_2 ($^1A_1$) along the non-least-motion path; two singlet methylenes dimerize via the non-least-motion path not to give a ground state but a Rydberg excited state of ethylene. The ground-state singlet SiH_2 dimerizes to form the ground state of disilene without barrier along the non-least-motion path and with substantial barrier along the least-motion path. In the case of silaethylene, the singlet methylene and the singlet silylene form the ground state of silaethylene without barrier along the non-least-motion path. The triplet methylene and the triplet silylene also form the ground state of silaethylene without barrier along the least-motion path.

Potential energy curves plotted as functions of the C–C, C–Si, or Si–Si distance change very much depending on the bond angles of CH_2 or SiH_2 fragment. The relative stability between the triplet × triplet electronic configuration and the singlet × singlet electronic configuration, which depends on the angles, determines the qualitative features of these potential curves. Schematic pictures of the potential curves in the least-motion path of dimerization reactions of XH_2 and YH_2 fragments to give disilene, silaethylene, and ethylene are shown in Figure 6 (X or Y is C or Si). The

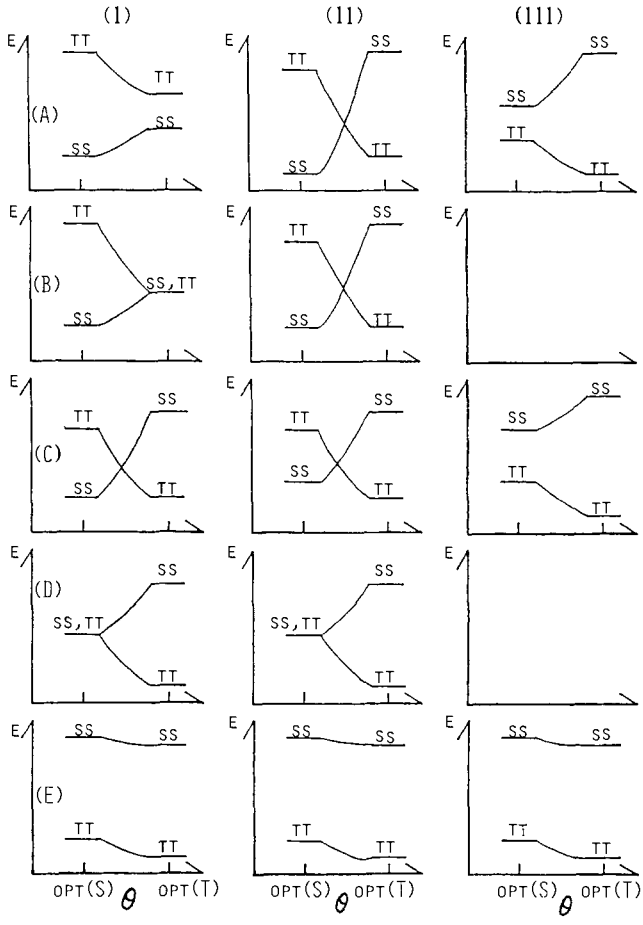

Figure 6. Schematic potential energy curves along the least-motion path for $XH_2 + YH_2 \rightarrow XH_2YH_2$ as functions of the bond angle ∠HXH = ∠HYH at various values of X–Y bond lengths: (I) for $SiH_2 + SiH_2$, (II) for $CH_2 + SiH_2$, and (III) for $CH_2 + CH_2$. R(Si–Si) is (I–A) ∞, (I–B) around 4.0 Å, (I–C) around 3.4 Å, (I–D) arund 3.1 Å, and (I–E) the product equilibrium distance. TT is the triplet × triplet and SS is the singlet × singlet electronic configuration. θ_{opt}(S) is an optimum bond angle for the singlet XH_2 fragment and θ_{opt}(T) is that of the triplet XH_2 fragment.

abscissa is the bond angle ∠HXH or ∠HYH and the ordinate is the total energy of the XH_2YH_2 molecule. SS represents the electronic configuration, singlet XH_2 × singlet YH_2, and TT denotes the electronic configuration, triplet XH_2 × triplet YH_2. Rydberg states are not considered here. Figures denoted by (I) show the case of disilene (X = Y = Si) at several Si–Si bond lengths. At R(Si–Si) = ∞, the SS configuration is always more stable than the TT at any angle between the optimum bond angle for singlet fragment θ_{opt}(S) and that of for triplet fragment θ_{opt}(T) (case I–A). Around R(Si–Si) = 4.0 Å SS and TT levels become equal in energy, i.e., a crossing of two configurations (an avoided crossing of two adiabatic surfaces) begins near θ_{opt}(T) (case I–B). The crossing occurs at smaller angles, between θ_{opt}(S) and θ_{opt}(T), around R(Si–Si) = 3.4 Å (case I–C). The last crossing occurs at θ_{opt}(S) around R(Si–Si) = 3.1 Å (case I–D). The TT surface is always under the SS surface between θ_{opt}(S) and θ_{opt}(T) at the equilibrium Si–Si bond length of disilene. In following cases I–A to I–E, one can qualitatively visualize the change of bond angles as the reaction proceeds. If the dimerization reaction starts from the SS configuration with small bond angle θ_{opt}(S) at R(Si–Si) = ∞, it should cross over the potential barrier to the TT surface at some R(Si–Si) between (I–B) and (I–D), by expanding the HSiH bond angles from θ_{opt}(S) to θ_{opt}(T), and arrive at the equilibrium geometry of disilene. Thus, the reaction coordinate of dimerization should be a mix between the bond length R(Si–Si) and the bond angles ∠HSiH. The case of CH_2SiH_2 is shown in Figure 6, case II. θ_{opt}(S) and θ_{opt}(T) of CH_2 are different from those of SiH_2. For qualitative consideration, however, no distinction has been made in this schematic potential picture. In this case, at R(C–Si) = ∞, there is already a crossing of the energy curves along the bond angle coordinate. This picture (II–A) corresponds to (I–C) of SiH_2SiH_2 at R(Si–Si) = 3.4 Å. If the dimerization path starts from the SS electronic configuration, it should cross over to the TT surface by expanding the bond angles with barrier before reaching to (II–D) and then arrive at the equilibrium geometry (II–E). On the other hand, if the reaction can start from TT at θ_{opt}(T), it will go to the product without a substantial change of bond angles and energy barrier. Figure 6, case III, is the case of CH_2CH_2. Even at R(C–C) = ∞, the TT surface is always more stable than the SS along the bond angle coordinate, and it leads to the equilibrium geometry of ethylene without any potential barrier.

In the case of the non-least-motion path, we have two more geometrical factors, ϕ_X and ϕ_Y, the bending angles of XH_2 and YH_2 fragments from the X–Y axis, respectively. Figure 6 is a special case where $\phi_X = \phi_Y = 0$. In the ground state along the non-least-motion path, there is no energy barrier for all of the three cases studied here.

Acknowledgment. The authors acknowledge Drs. Y. Osamura and M. Dupuis for their valuable advice in using the GAMESS program. E.R.D. was Visiting Professor at IMS when the work presented here was carried out. Numerical calculations were carried out at the Computer Center of IMS.

Registry No. CH_2, 2465-56-7; SiH_2, 13825-90-6; CH_2CH_2, 74-85-1; SiH_2SiH_2, 15435-77-5; CH_2SiH_2, 51067-84-6.